THE JOURNAL OF PHYSICAL CHEMISTRY C
A JOURNAL OF THE AMERICAN CHEMICAL SOCIETY

pubs.acs.org/JPCC

Article

Microscale Thermophoresis in Liquids Induced by Plasmonic Heating and Characterized by Phase and Fluorescence Microscopies

Sadman Shakib, Benoit Rogez, Samira Khadir, Julien Polleux, Alois Würger, and Guillaume Baffou*

Cite This: J. Phys. Chem. C 2021, 125, 21533–21542

Read Online

ACCESS | Metrics & More | Article Recommendations | Supporting Information

ABSTRACT: Thermophoresis denotes the motion of particles along temperature gradients. Insignificant in most daily-life observations, this peculiar effect can become dominant in applications involving nano- and microscale heating in fluids. Recent studies in nanoplasmonics observed significant thermophoresis of molecules and particles, in particular in plasmonic trapping, SERS, and biosensing. Evidencing the presence of thermophoresis is not obvious and quantifying its magnitude is even less accessible considering existing techniques. In this article, we introduce a method capable of quantifying the thermophoresis of particles in the context of nanoplasmonic applications. A gold nanoparticle array under illumination is used to create microscale temperature gradients, and a dual fluorescence-phase microscopy technique is used to map both temperature and concentration in parallel. This association enables the determination of Soret coefficients for a wide range of temperatures from a single image acquisition. This metrology technique paves the way for broader fundamental research in microscale thermophoresis in liquids and better-controlled applications in nanophotonics involving thermoplasmonic effects.

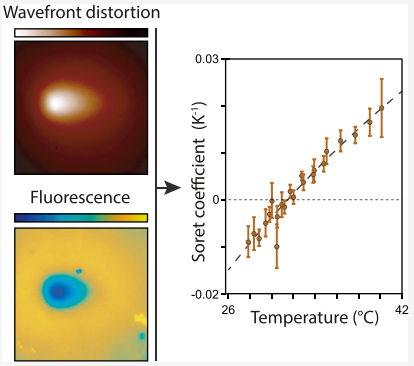

INTRODUCTION

When a temperature gradient is applied throughout a fluid, dissolved species (solute) tend to move along the thermal gradient (usually from hot to cold), even when the fluid remains static. This effect is called thermophoresis. While thermophoresis is well understood in gases, thermophoresis in liquids is more complex, especially in water, originating from multiple processes, e.g., Seebeck effect, thermoosmosis, van der Waals interactions, thermal diffusion, etc. Thermophoresis is a tenuous process, usually overwhelmed by thermally induced convection if no caution is used. Two kinds of solutes are usually considered: (i) microparticles, the motion of which can be studied by particle tracking and where the readouts are positions (x_i, y_i), and (ii) molecules, where the physical quantity of interest is a concentration field $c(x, y)$ featuring deviation from uniformity. Experimental investigations of thermophoresis are made much easier at small scales because huge temperature gradients can be generated (around $\sim 10^6$ K·m^{-1} at the microscale), making thermophoresis much faster and dominant over other dynamical processes.

Microscale thermophoresis in liquids (MTL) is now at the basis of important applications. In particular, since 2010, NanoTemper Technologies GmbH has been using thermophoresis and its characterization with fluorescence imaging to quantify biomolecular affinity[1,2] or protein stability,[3,4] since the modification or the association of biomolecules, such as proteins, can dramatically modify their thermophoretic properties. The success of this company, which now employs around 150 people, highlights the high degree of applicability of microscale thermophoresis today. In parallel, more fundamental research has been carried out, in particular by shining gold nanoparticles to create localized temperature gradients at the nano/microscales. Metal nanoparticles can behave as efficient light absorbers when illuminated at their plasmonic resonance wavelength, lying from the visible to near-infrared range for gold. This picture is at the basis of the field of research named thermoplasmonics.[5,6] Having an absorbance of the sample confined in the infrared region is particularly interesting as it enables the sample to remain transparent in the visible range, making any further optical characterization of the system easier, for instance, using fluorescence.[7] Several groups have been particularly active on using thermoplasmonic approaches to thermophoresis experiments, in particular to achieve trapping of biomolecules using adaptive microscale temperature gradients,[8−10] trapping of quantum dots,[11] and multiple trapping of plasmonic nanoparticles.[12] Plasmonics-assisted thermophoresis was also proven efficient for nanofabrication purposes.[13,14] Also, a strong interest was born in the 2010s for the study of the so-called Janus nanoparticles.[15,16] When dielectric nanospheres are covered by a hemispherical metallic cap, they exhibit a thermophoresis-assisted unidirectional fast motion under illumination. Recently, unexpected thermopho-

Received: July 15, 2021
Revised: September 8, 2021
Published: September 22, 2021

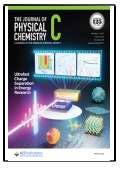

https://doi.org/10.1021/acs.jpcc.1c06299
J. Phys. Chem. C 2021, 125, 21533−21542

resis was observed to have a dominant effect, either positive or detrimental, for studies in optical trapping,[17] surface-enhanced Raman scattering (SERS),[18] optical printing,[19] and plasmonic sensing.[20,21] The interest of plasmonics in the study of MTL is now established, promising, and increasing. In this field, the main difficulty remains the estimation of the local microscale temperature gradients.

Metrology in MTL gained interest in the 2000s, following the invention of several optical characterization techniques that enabled the accurate measurements of Soret coefficients S_T and thermophoretic mobility D_T (see definitions further on). The oldest one is the beam deflection technique,[22−25] where deflection of a laser beam passing through macroscopic thick liquid occurs due to the refractive index (RI) variations originating from transverse temperature and concentration gradients. Temperature and concentration contributions can be distinguished because they occur over different time scales, thermal diffusion being much faster than thermophoretic transport. Forced Rayleigh scattering is another RI-based technique,[26] which enables the measurement of both S_T and D_T. Interferences between two tilted laser beams produce parallel fringes, leading to a spatially periodic temperature grating due to the absorption of a dye layer on a surface. This technique has been applied to investigate aqueous binary mixtures,[27] polymer solutions,[28] and colloidal suspensions.[29] Temperature-induced RI variation in liquids can also yield a thermal lensing effect, a phenomenon at the basis of another characterization technique.[30] In this approach, laser heating occurs via the direct absorption of infrared light (980 nm) by water. All of these techniques, based on thermally induced RI variations, are often slow due to the large size of the system (above 100 μm), leading to strong inertia; they quantitatively measure neither the temperature nor the concentration; and they require a large solute concentration (around 1 wt %).

To solve these problems, a fluorescence microscopy approach was developed.[31−33] The solute of interest was fluorescently labeled, enabling the investigation of weaker concentrations, and laser heating was applied through the objective lens of a microscope, over a micrometric area, making thermophoresis processes faster. While fluorescence images acquired using a fluorescence microscope can directly provide quantitative measurements of concentration gradients, measuring the microscale temperature remains complicated. For this purpose, the technique uses an additional, thermosensitive fluorophore dispersed in the liquid, associated with another spectral range, enabling the parallel mapping of the microscale temperature distribution. However, this second approach suffers from known artifacts: the temperature is measured through fluorescence intensity of some dispersed molecules in the liquid, but these molecules can undergo thermophoresis as well, making the fluorescence intensity not only dependent on temperature: the fluorescence decay observed where the laser is focused can arise from a temperature decrease, but also from a molecular depletion or accumulation. Then, the fluorescence intensity for the solute, supposed to render the concentration, may be temperature-dependent, making the intensity not a faithful indication of the concentration. The authors themselves confessed possible artifacts up to 8%,[32] which is certainly a lower limit.

In this article, we introduce a metrology technique for MTL characterization using fluorescence mapping for concentration measurements and quantitative phase microscopy for temperature measurements. This association enables one to keep all of the benefits of microscale fluorescence characterization (rapidity, low solute concentration) and to discard possible artifacts thanks to the label-free mapping of the temperature distribution. We also introduce the use of gold nanoparticles as effective light absorbers and the spatial reshaping of the light beam to achieve controlled, well-defined microscale temperature gradients. We illustrate the principle of this approach on the simple case of 28 nm fluorescent beads in pure water.

THERMOPHORESIS

In a liquid at rest (no convection) containing a solute of concentration c, the solute flux density $\mathbf{J}$ reads

$$\mathbf{J}(\mathbf{r}, t) = -D\nabla c(\mathbf{r}, t) - c(\mathbf{r}, t)D_T\nabla T(\mathbf{r}, t) \quad (1)$$

where T is the temperature, D is the solute diffusion coefficient, and D_T is the solute thermophoretic mobility. This equation assumes small concentration (weight fraction $\ll$1 wt %), where D_T and D are independent of concentration; yet they do depend on temperature. The first term on the right-hand side of eq 1 depicts the solute diffusion (Fick's law), and the second term denotes thermophoresis. In the steady state, the particle current vanishes, $\mathbf{J} = \mathbf{0}$, resulting in the relation

$$\nabla \ln c = -S_T\nabla T \quad (2)$$

where the Soret coefficient is defined as $S_T = D_T/D$, i.e., the ratio of two transport coefficients. While D_T tells how fast a solute migrates along a temperature gradient, S_T is rather related to the magnitude of solute depletion or accumulation in the steady state around a hot spot. The Soret equilibrium (eq 2) thus describes the competition of thermodiffusion (which tends to create an out-of-equilibrium solute gradient) and Brownian motion (which tends to homogenize the concentration).

In the last two decades, Soret coefficients of various molecular and colloidal systems have been measured.[34−36] Although particles suspended in a gas phase always move toward the cold ($S_T > 0$), this rule does not always apply in aqueous dispersions. For instance, a change of sign of the Soret coefficient has been observed upon adding a small amount of polymer,[37] modifying the composition of the electrolyte,[38,39] or lowering the temperature.[35,40] For many solutes, the temperature dependence of the Soret coefficient follows the empirical expression proposed by Piazza[40]

$$S_T(T) = S_T^\infty\left[1 - \exp\left(\frac{T^* - T}{T_0}\right)\right] \quad (3)$$

which denotes a change of sign of the Soret coefficient at a temperature T^*, and where S_T^∞ and T_0 are constants, as represented in Figure 1.

Note that the slope of S_T at $T = T^*$ is simply $S'_T(T^*) = S_T^\infty/T_0$.

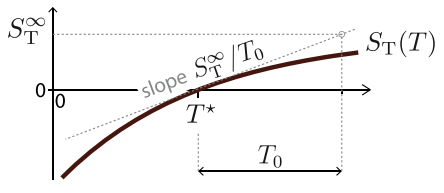

Figure 1. Plot of eq 3 and meanings of all parameters: S_T^∞, T^*, and T_0.

https://doi.org/10.1021/acs.jpcc.1c06299
J. Phys. Chem. C 2021, 125, 21533−21542

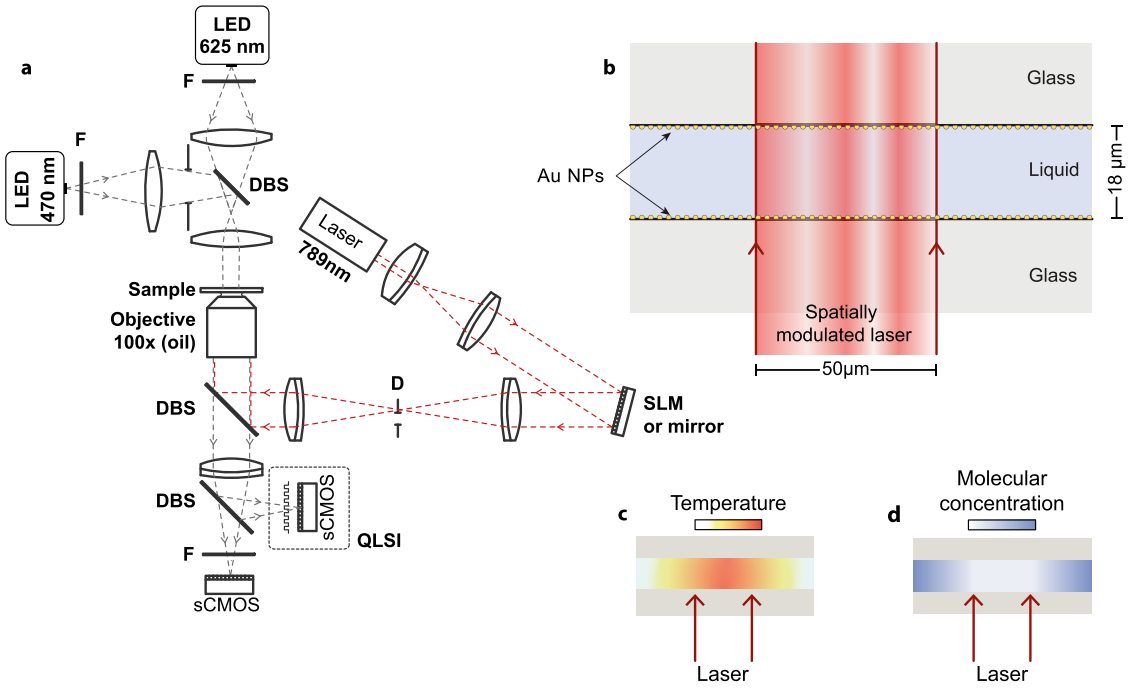

Figure 2. (a) Schematic of the microscope. DBS: Dichroic beam splitter. D: diaphragm. F: filter. (b) Schematic of the sample. Gold nanoparticle-deposited coverglasses are used to create a sandwiched geometry. (c) Schematic of the temperature gradient resulting from laser heating of the gold nanoparticles. (d) Schematic of the concentration gradient resulting from the temperature gradient.

Depending on solute and solvent properties (hydrophobicity, ionicity, pH, etc), T^* typically varies from 4 to 30°C while S_T^∞ is on the order of 10^{-2} K^{-1}. The origin of this empirical law is not understood. This temperature dependence resembles that of the thermal expansivity of water or the inverse of water viscosity. Yet, so far no sound relation to any of these quantities has been established.

The current understanding of thermophoresis was introduced by Derjaguin in 1941: Due to interactions with a solid, the heat or enthalpy content of the liquid close to the surface is usually lower than in the bulk. According to the second law, heat flows to the cold. Close to the particle surface, heat diffusion is supplemented by advection of low-enthalpy liquid to the hot. This effect, called thermoosmosis, can be rationalized by balancing thermally induced and viscous stresses,[41−43] and has been observed experimentally by visualizing the creep flow in a microchannel.[44] Similarly, a suspended particle pumps the surrounding liquid to the hot, and by reaction moves in the opposite direction. Some dependencies on material properties have been worked out in detail, such as the fact that D_T is independent of the particle size,[41] the role of permittivity and salinity gradients for the electrostatic double-layer forces,[39] and specific-ion effects.[45]

The physical mechanism underlying the empirical law (eq 3) appears to be a key problem for a better understanding of colloidal thermophoresis. Thus, theoretical investigations in MTL ideally require Soret data over a wide range of temperatures to fully characterize the system, which is usually time-consuming given the slowness of thermophoretic processes.

EXPERIMENTAL METHOD

We introduce here an experimental approach for Soret coefficient measurement in MTL based on the use of an optical microscope, to study small systems featuring fast dynamics. Two optical microscopy techniques are used in parallel: Fluorescence microscopy is used for concentration mapping, and quantitative phase microscopy is used for temperature mapping. Heating is performed by illuminating gold nanoparticles with a 789 nm laser beam reshaped by a spatial light modulator, to achieve controlled temperature gradients. Let us describe in more detail all of these aspects of the methodology.

Setup Geometry. The experimental setup is a homemade microscope that combines fluorescence and quantitative phase microscopies (Figure 2a). Sample fluorescence was excited from the top of the sample, using an LED at 470 nm (M470L3, Thorlabs, 650 mW), and collected using an sCMOS camera (ORCA Flash 4.0 V3, 16-bit mode, Hamamatsu). Quantitative phase microscopy (QPM) was performed using an LED illumination at 625 nm (M625L3, Thorlabs, 700 mW) and a quadriwave lateral shearing interferometry (QLSI) camera (Sid4-sC8, Phasics SA).[46,47] We recently proposed to rechristen this technique in cross-grating phase microscopy.[48] This QPM technique is simply based on the association of a regular camera (Zyla 5.5, Andor) with a two-dimensional diffraction grating, positioned at a millimetric distance from the camera sensor. The recorded image (called an interferogram) was processed to quantitatively retrieve the optical wavefront distortion caused by the sample.

A wavelength-tunable, titanium:sapphire laser (laser Verdi G10, 532 nm, 10 W, pumping a Tsunami laser cavity, Spectraphysics), set at a wavelength of 789 nm, was used to heat the sample at the microscale. Before entering the objective lens of the microscope, the laser beam was reshaped using a spatial light modulator (SLM) (1920 × 1152 pixels, Meadowlark Optics), acting on the phase spatial profile of the laser. The SLM eases the measurements and the S_T retrieval algorithm by creating a linear temperature profile. However, the SLM can also be replaced by a mirror, which would yield a

https://doi.org/10.1021/acs.jpcc.1c06299
J. Phys. Chem. C 2021, 125, 21533−21542

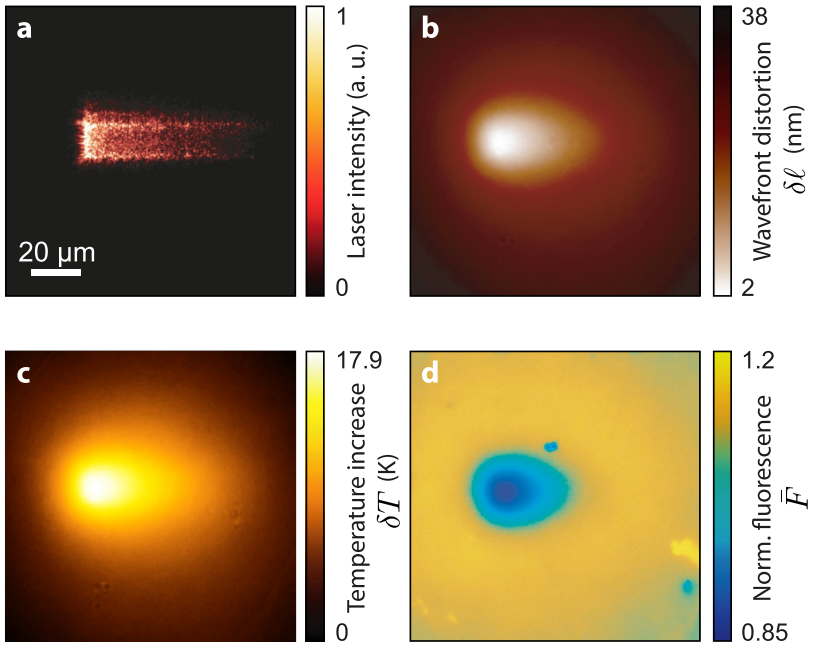

Figure 3. (a) Intensity profile of the laser beam at the sample plane. (b) Wavefront distortion stemming from the liquid heating by the laser, and its subsequent RI variation. (c) Map of the temperature increase, retrieved from image (b). (d) Variation of the fluorescence intensity $\delta F = F - F_0$.

Gaussian-like temperature profile, from which the measurements can also be performed with good accuracy, although over a more restricted spatial extension.

Sample Geometry. We focused on the study of the thermophoresis of 28 nm carboxylated fluorescent nanobeads (yellow-green (505/515) FluoSpheres, F8888, Thermo Fisher) in pure water (collected from a Milli-Q system), diluted at a concentration of c_∞ = 88 nM, i.e., a volume fraction of 0.061 vol %. A 7 μL drop of solution was pressed between two circular glass coverslips (18 and 25 mm in diameter); 15 μm beads at a concentration of 8.2 fM were added in the solution to achieve a controlled liquid thickness h, found to be around 18 μm (Figure 2b) in practice. The coverslips were previously treated within an air-plasma chamber to increase the hydrophilicity of the glass surfaces, favoring the drop spreading and a thin water layer. This small layer thickness is meant to avoid thermoconvection and ensures a uniform temperature profile along the vertical direction, making T dependent only on the radial coordinate in the fluid. To avoid evaporation, the top of the Attofluor chamber was covered by a 25 mm coverslip and sealed with a paste that polymerizes once mixed (Picodent). This sandwich structure was mounted in an Attofluor metallic cell chamber (Thermo Fisher).

Both glass coverslips were coated with gold nanoparticles to improve the temperature uniformity along the vertical direction. The gold nanoparticle samples were made by block copolymer micellar lithography (BCML).[49] BCML enables the easy and cost-effective deposition of gold nanoparticles on a whole glass substrate with a quasi-periodic hexagonal distribution, and with nanoparticle interdistance of typically 50−100 nm. The nanoparticle morphology can be modified to shift the plasmonic resonance from around 530 nm to the infrared. The plasmonic resonance of the samples we used was around 800 nm. The fabrication procedure and sample characterization are detailed in Supporting Information Section A.

Heating could also be performed using a simple absorbing layer, like a thin chromium layer.[50] However, a chromium layer would uniformly absorb over the whole visible spectral range. A layer absorbing mostly in the red/infrared region of the spectrum and being more transparent in the visible range, like these plasmonic nanoparticles samples, is preferred because it avoids absorption of the emitted fluorescence. The other benefit of using a discontinuous metal layer is that it avoids thermal diffusion along the metal layer. Because metals are highly conductive, the temperature distribution could spread and prevent localized heating within the field of view of the microscope. Note that despite the nanometric size of the heat sources, the temperature is perfectly smooth at the microscale due to thermal collective effects.[51]

The liquid thickness h was measured by making the focus on the top and then on bottom water/glass interfaces using a piezo microscope holder (pifocFast PIFOC, PI), and measuring the resulting translation δz of the objective lens along z. Then, h was obtained by applying the correction $h = \frac{n_{\text{liquid}}}{n_{\text{air}}}\delta z$ (at room temperature, without laser heating).[52]

Laser and Temperature Shaping. A collimated laser sent to the back aperture of an objective lens normally produces a diffraction-limited focalized spot at the imaged plane. However, by engineering the phase profile of the laser at the back aperture of the objective, it is possible to create any light intensity profile at the imaged plane. The phase profile to be applied can be calculated using a Gerchberg−Saxton algorithm.[53,54] The phase profile of the light beam is modified using a spatial light modulator (SLM). In practice, the SLM cannot be placed at the entrance pupil of the objective lens, for space reasons. It is thus remotely positioned at a place that is conjugated with the entrance pupil using a 4-f arrangement (Figure 2a). This 4-f configuration also enables the zero-order spot to be removed by a diaphragm (D, in Figure 2a).

In the methodology introduced here, light shaping is used to shape the temperature profile (Figure 3). In particular, we shaped the laser beam (Figure 3a) to achieve a perfect linear

https://doi.org/10.1021/acs.jpcc.1c06299
J. Phys. Chem. C 2021, 125, 21533−21542

temperature gradient over a rectangular area (Figure 3c). The determination of the light profile to achieve a given temperature is not straightforward. It requires an inversion algorithm, described in refs 53, 55. As detailed further on, setting a linear temperature gradient over the field of view of the microscope enables the straightforward determination of $S_T(T)$ over a large range of temperatures, from a single image acquisition.

Temperature Imaging Using Wavefront Sensing. The temperature increase throughout the fluid, resulting from the heating of the gold nanoparticles using the laser illumination (Figures 2c and 3c), gives rise to a refractive index (RI) variation δn. Just like the temperature field, δn is also considered as uniform over the vertical direction, and can be considered as only dependent on the x and y coordinates: $\delta n(x,y)$. To retrieve the temperature map, we measure this wavefront distortion using QPM.[56] This RI variation distorts the incoming planar wavefront of the probe beam crossing the sample (LED at 625 nm) (Figure 3b). This distortion created by this thermal lens effect reads

$$\delta l(x, y) = h\,[n(x, y) - n_\infty] \tag{4}$$

where $n(x,y)$ is the refractive index map of the liquid upon laser heating and n_∞ is the refractive index of the liquid at ambient temperature T_∞. In first approximation, for small temperature increases (typically below 20 K), the refractive index of water varies linearly with temperature, $n(T) = n_\infty + \beta\delta T$, and one can easily determine the temperature from the wavefront distortion image using

$$\delta T(x, y) = \frac{\delta l(x, y)}{h\beta} \tag{5}$$

where $\delta T = T - T_\infty$ (Figure 3c). However, in this study and in general in MTL experiments, the temperature increase can exceed 20 K. In that case, the nonlinear $n(T)$ function of the liquid has to be considered. For water, data sets can easily be found in the literature.[57] For other liquids, $n(T)$ can be also measured by cross-grating phase microscopy, with a microvessel containing the liquid.[58] Such a vessel can be a microcrater made by CO_2 laser micro-ablation of the surface of a glass slide. For water, as $n(T)$ is a monotonic function, it can be numerically inverted to get the $T(n)$ calibration function (see the Supporting Information for more details) and retrieve the temperature map $T(n(x, y))$ directly from the refractive index map $n(x, y) = n_0 + \delta l(x, y)/h$.

Concentration Imaging Using Fluorescence Microscopy. The temperature gradient results in a concentration gradient, following Figure 2c,d. Mapping of the solute concentration was done using fluorescence microscopy. Fluorescence signal is proportional to concentration only in first approximation. For instance, subtracting the camera offset value is important (111 counts, in our case), but not the only caution to be used. The general relation between fluorescence F and concentration c can be written, in the context of our study, as

$$F = \alpha(T) I_0 c \tag{6}$$

where I_0 is the excitation light intensity and $\alpha(T)$ is a parameter that expresses the collection efficiency of the microscope, and also the brightness of the fluorescent compound, the latter usually being temperature-dependent (usually decreases with temperature). Let $F_0(x,y)$ be the fluorescence intensity image measured without laser heating, i.e., at uniform temperature T_∞ (and thus at uniform concentration c_∞). From eq 6, one can write

$$F_0(x, y) = \alpha(T_\infty) I_0(x, y) c_\infty \tag{7}$$

Even under wide-field illumination, I_0 is never perfectly uniform, hence its spatial dependence. With laser heating, the fluorescence intensity image $F(x, y)$ becomes

$$F(x, y) = \alpha(T(x, y)) I_0(x, y) c(x, y) \tag{8}$$

By dividing (8) by (7), one ends up with

$$\frac{c(x, y)}{c_\infty} = \frac{\alpha(T)}{\alpha(T_\infty)} \frac{F(x, y)}{F_0(x, y)} \tag{9}$$

which can be recast into

$$c(x, y) = c_\infty \bar{\alpha}(T(x, y)) \bar{F}(x, y) \tag{10}$$

where $\bar{F} = F/F_0$ is the normalized fluorescence intensity image and $\bar{\alpha}(T) = \alpha(T)/\alpha(T_\infty)$ is the temperature-dependent correction factor of the fluorescence brightness. This relation is the general expression used to calculate the concentration image from the fluorescence image. $\bar{\alpha}(T)$ can be easily measured experimentally, either in a fluorimeter with temperature control or within the microscope setup, if it is equipped with a heating stage. We opted for the latter option (using the VAHEAT system from Interherence).

Some other complications may occur. In particular, eq 10 assumes neither photobleaching nor thermobleaching occurs. For the fluorescent particles we used, these effects have been quantified, and found to be negligible (see the Supporting Information). In particular, the use of beads instead of molecules favors good fluorescence stability.

However, photobleaching is not supposed to be problematic in this procedure and to affect the determination of S_T, anyway. If the illumination is uniform, photobleaching occurs over the whole field of view with a uniform decay. But multiplying the concentration field with a uniform time-dependent factor $\alpha(t)$ does not change the quantity $\nabla\ln(c)$ in eqs 2 and 10, since $\nabla\ln(\alpha c(\mathbf{r})) = \nabla[\ln(\alpha) + \ln(c(\mathbf{r}))] = \nabla\ln(c(\mathbf{r}))$. Thus, photobleaching itself is not an issue. Note that this benefit no longer holds when using fluorescence intensity to probe temperature (not concentration) as reported in other studies,[32] since no logarithm is involved in the denominator of eq 11: $\nabla T(\mathbf{r})$, hence the interest of going without fluorescence for temperature metrology in MTL, as we propose here. Note that photobleaching is not a problem as long as it is not temperature-dependent. But usually, photobleaching is accelerated when increasing the temperature, which may yield a nonuniform $\alpha(\mathbf{r},t)$ value over the field of view, and the benefit of the logarithm is lost. Equally, thermobleaching remains an issue if it is significant, since it does not affect fluorescence uniformly over the field of view. To minimize the effect of thermobleaching, the acquisition length of the measurements has to be shortened accordingly, to ensure $\alpha(\mathbf{r}, t) \approx \alpha_0$. This would lead to a poorer signal-to-noise ratio. To compensate for this limitation, the fluorescence excitation light intensity can be increased, even at the expense of photobleaching, since photobleaching is not an issue for the reason mentioned above. In our experiments, both thermobleaching and temperature dependence of photobleaching were quantified and proved insignificant, as shown in the Supporting Information.

https://doi.org/10.1021/acs.jpcc.1c06299
J. Phys. Chem. C 2021, 125, 21533−21542

S_T RETRIEVAL PROCEDURE

Basic Principle. The determination of both a temperature gradient and the resulting concentration gradient permits the determination of the Soret coefficient at the temperature $T(x,y)$, according to eq 2, which can be recast using eq 10

$$S_T(T(x,y)) = -\frac{\nabla \ln \overline{F}(x,y)}{\nabla T(x,y)} \tag{11}$$

Note that this expression involves the division by a vector, which is not mathematically defined. However, in the steady state, $\nabla \ln \overline{F}$ and ∇T are necessarily colinear anywhere in space. Therefore, the gradients can be understood as scalar gradients along the direction of ∇T.

Equation 11 reveals the possibility to measure a large set of S_T coefficients for various temperatures, from a single image acquisition, ideally one S_T value per pixel (x, y). However, in practice, some caution has to be used. First, ∇T, appearing in the denominator of eq 11, can be very small and even reach zero in some parts of the image, e.g., around the maximum temperature location and far from the heat source. These areas cannot give reliable S_T estimations. To reduce these issues, measurements have to be taken only where temperature profiles are sloping. To ease the measurements, we applied a linear temperature gradient, over a rectangular area $\mathcal{R}$ of the field of view, by SLM laser beam shaping (Figure 3a). Then, all of the S_T values were estimated over this area where the temperature gradient (Figure 3c) is easy to process and where it does not feature problematic values close to zero. The $\overline{F}(x)$ and $T(x)$ horizontal profiles were calculated by averaging over the vertical lines of $\mathcal{R}$ to improve the signal-to-noise ratio.

Second, the unavoidable noise on each profile ($\overline{F}(x)$ and $T(x)$), even small, can result in dramatic noise once the image *derivatives* are calculated. To get around this problem, we divided $\ln F(x)$ and $T(x)$ into m sections of 6 μm length and fit all data points inside each section using a linear regression model. The corresponding slopes of each of the m sections of $T(x)$ and $\ln F(x)$ are used to calculate m values of S_T at m different temperatures according to eq 11.

Managing the Time Scales. Equation 11 (derived from eq 2) is valid only in the steady state, which imposes a delay, after heating is turned on, before acquiring consistent images.

Three time scales come into play. The first one is the thermal diffusion time

$$\tau_{th} = L^2/a \tag{12}$$

where L is the characteristic size of the heat source and a is the thermal diffusivity of the medium. In the present system, the characteristic size of the laser beam at the sample plane is around 50 μm and $a \sim 10^{-7}$ m^2·s^{-1} for both glass and water, resulting in a time scale on the order of $\tau_{th} \sim 10$ ms, much faster than any measurement than can be performed here. Thus, one can consider that the temperature steady state appears instantaneously when the laser is turned on, and vanishes as fast, when the laser is turned off.

The second time scale characterizes the solute diffusion in the liquid following a perturbation over the spatial scale L, and reads

$$\tau_c = L^2/D \tag{13}$$

For 28 nm spheres, the Stokes−Einstein relation gives $D \sim 10^{-11}$ m^2·s^{-1}, leading to $\tau_c \sim 1$ s. The evolution of the concentration is thus much slower than the temperature. Note that if the heating size was in the millimetric range, it would yield a time scale on the order of several hours or even days, highlighting the interest of using a microscopy approach to study MTL. This time scale is the one observed in our experiments (see further on).

There is a third time scale, also arising from eq 1, that is worth discussing. It is the time scale τ_T associated with the thermophoretic mobility D_T, and scaling as $L^2/\langle\delta T\rangle D_T = \tau_c/S_T\langle\delta T\rangle$ where $\langle\delta T\rangle$ is the typical temperature variation occurring over the distance L (a few tens of degrees maximum in our case). τ_T is the time required for a particle to drift along a distance L by thermophoresis. Since S_T is usually on the order of 10^{-2} K^{-1}, τ_T was typically 10 times larger than τ_c in our study, making τ_c the dominant (since smaller means faster) time scale.

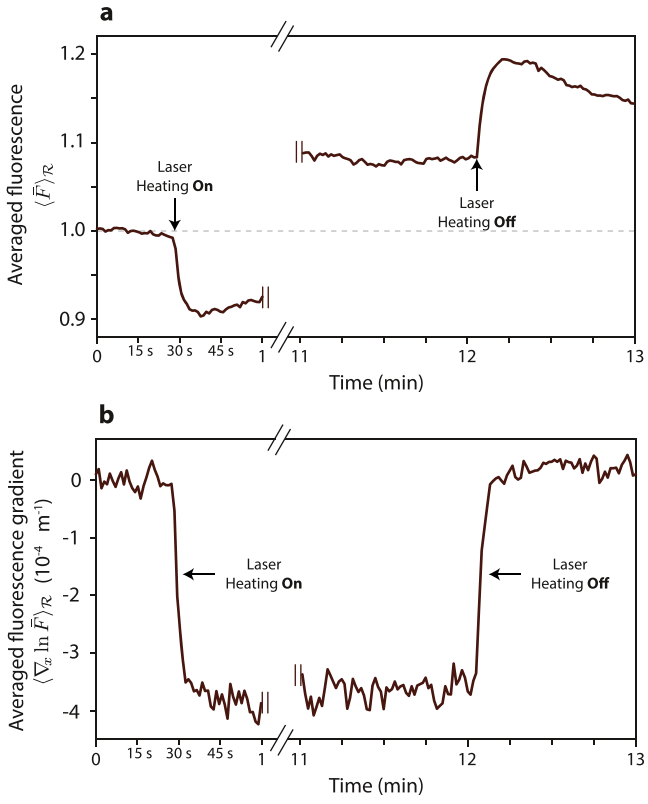

Figure 4. (a) Temporal evolution of the average fluorescence in the temperature gradient throughout a long experiment. Fluorescence is increasing with time as nanobeads are accumulating with time. (b) Associated temporal evolution of $\frac{d}{dx}[\ln F(x)]$, cancelling the slow fluorescence increase $\frac{d}{dx}[\ln F(x)]$.

Figure 4a plots the temporal evolution of the image fluorescence, averaged over $\mathcal{R}$, $\langle \overline{F} \rangle_{\mathcal{R}}$. Once the laser is turned on, the fluorescence drops suddenly, over a few seconds, consistent with the estimation of τ_c above. This is the depletion of fluorescence due to beads escaping the hot spot by thermophoresis, tempered by the Brownian motion and natural molecular diffusion. However, the whole $\mathcal{R}$ area exhibits a subsequent, much slower, overall fluorescence increase until a steady state is reached after a few minutes. This increase is due to beads migrating from much further,

https://doi.org/10.1021/acs.jpcc.1c06299
J. Phys. Chem. C 2021, 125, 21533−21542

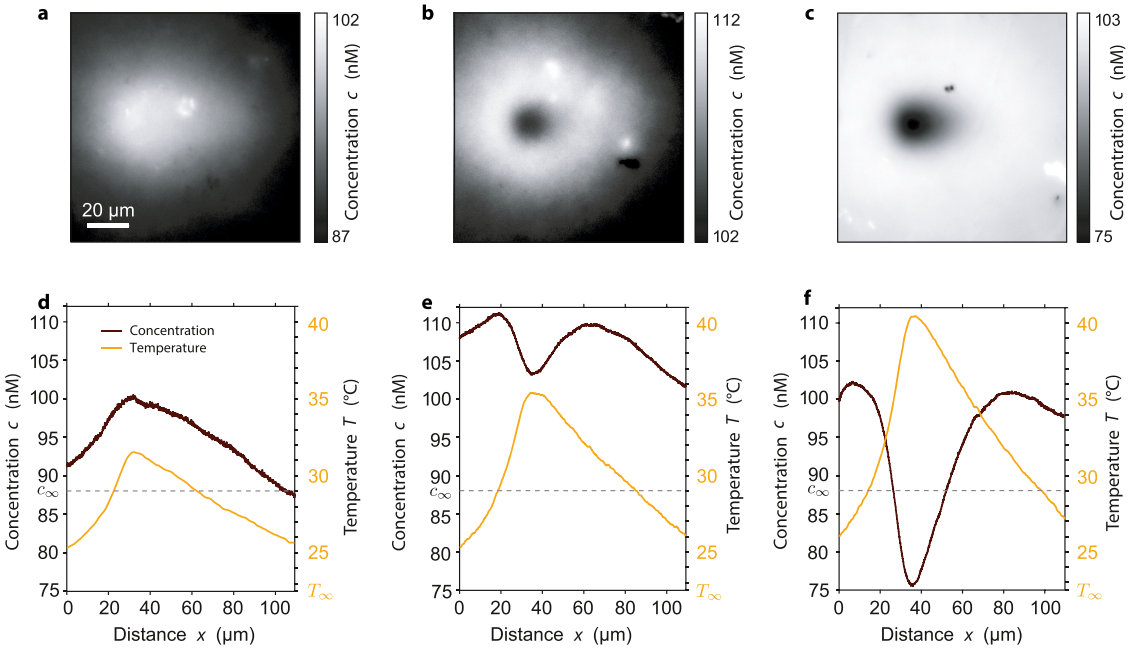

Figure 5. (a) Concentration image, for the lowest power P_{laser} = 5.22 mW, computed using eq 10 from the fluorescence image. (b) Same as (a) for P_{laser} = 8.25 mW. (c) Same as (a) for P_{laser} = 11.7 mW. (d) Concentration profile of image (a), i.e., for P_{laser} = 5.22 mW, averaged over 33 horizontal lines of the image (black curve), and associated the temperature profile (orange curve). (e) Concentration profile of image (b), i.e., for P_{laser} = 8.25 mW, averaged over 105 horizontal lines of the image (black curve), and associated the temperature profile (orange curve). (f) Concentration profile of image (c), i.e., for P_{laser} = 11.7 mW, averaged over 105 horizontal lines of the image (black curve), and associated the temperature profile (orange curve).

where the temperature gradient is very small, and thus the particle migration very slow. This slow migration from very far contributes to populate the area of interest with solute. However, luckily enough, the logarithm of eq 11 cancels this effect, since an overall increase of $\overline{F}(x,y)$ by a constant factor only yields an offset of $\ln \overline{F}(x,y)$, which is canceled when considering $\nabla \ln \overline{F}(x,y)$. As a demonstration, Figure 4b plots $\langle \nabla_x \ln \overline{F} \rangle_{\mathcal{R}}$ over time and, in accordance with this reasoning, the related steady state is reached after a few seconds only.

The main and important conclusion is that, although the concentration did not reach the steady state within the area of interest, quantitative measurement can still be achieved, which normally occurs after a few seconds using microscopy means. As a consequence, with the methodology we propose here, a full set of S_T measurement can be achieved in a few seconds. This short time scale of experiment also contributes to reduce possible photo- and thermobleaching problems. Of course, longer acquisitions of images can be performed once the steady state is reached, over seconds or even minutes to improve the signal-to-noise ratio, within the limit of what photo- and thermobleaching enables.

EXPERIMENTAL RESULTS

To illustrate the methodology, we conducted experiments on the thermophoresis of carboxylated fluorescent 28 nm nanobeads in pure water. Temperature and fluorescence images were acquired for three different laser powers, leading to maximum temperatures of 31.5, 35.5, and 40.5 °C. The resulting concentration images are displayed in Figure 5. When the temperature does not exceed 31.5 °C, a fluorescence accumulation is observed at the hot spot (Figure 5a), revealing a thermophilic effect of the nanobeads, i.e., a negative Soret coefficient. At higher temperatures, the opposite effect occurs (Figure 5b,c). A fluorescence depletion appears on top of the fluorescence accumulation, demonstrating a thermophobic effect at higher temperatures and a reversal of the sign of the Soret coefficient, in agreement with the empirical law (3). Figure 5d–f plots the temperature and concentration profiles, averaged over ∼100 horizontal lines (around 5.5 μm) in the center of the image. These line shapes are then processed to retrieve the Soret coefficients as a function of the longitudinal coordinate $S_T(x)$. Then, the coordinate x is converted into temperature using the $T(x)$ measured relation, to plot $S_T(T)$. Results are displayed in Figure 6, which plots the processed S_T values in the three cases presented above, covering three temperature ranges, and evidencing consistent measurements with each other. This $S_T(T)$ profile is in full agreement with what was previously reported in the literature, in particular by Putnam and co-workers, who studied 26 nm carboxylated beads in water.[25] The fit of the measurements using eq 3 is represented using a dashed line and gives T^* = 31.5 ± 0.2, T_0 = 35 ± 41 °C, and S_T^∞ = 0.09 ± 0.1 K^{-1}. The error bars on T_0 and S_T^∞ are large, despite the good fit of the experimental data. This issue is due to the fact that this set of three parameters is not ideal. A fitting parameter that should be much better defined is rather the slope of the S_T profile, which is equal to $S_T'(T^*) = S_T^\infty/T_0$ at $T = T^*$ (see Figure 1). Thus, let us discard T_0 and rather use the parameter $S_T^\infty/T_0 \triangleq s_T^*$ to get a more natural and intuitive association of fitting parameters. In this case, one can recast the S_T expression (3) as

$$S_T(T) = S_T^\infty \left[1 - \exp\left(s_T^* \frac{T^* - T}{S_T^\infty}\right)\right] \tag{14}$$

With this new set of three fitting parameters, one gets T^* = 31.5 ± 0.2 °C, s_T^* = 0.00253 ± 0.00021 K^{-2}, and S_T^∞ = 0.09 ±

https://doi.org/10.1021/acs.jpcc.1c06299
J. Phys. Chem. C 2021, 125, 21533−21542

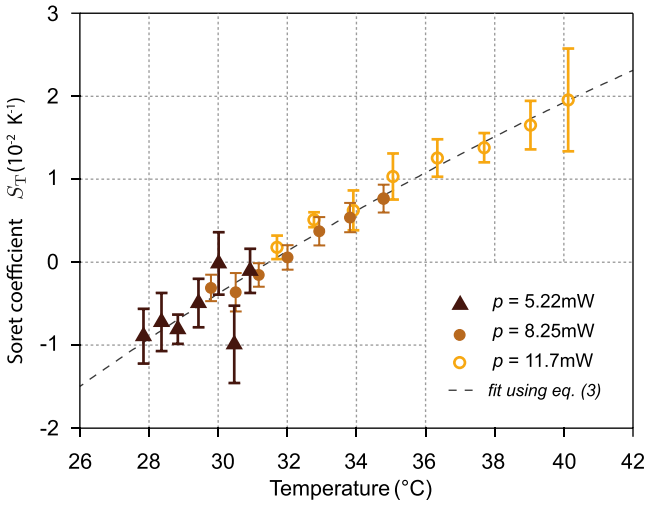

Figure 6. Three series of Soret coefficients, measured from three video acquisitions at laser powers 5.22 mW (brown triangle), 8.25 mW (yellow filled circle), and 11.7 mW (yellow open circle). The dashed line represents a fit of all this experimental data using eq 3.

0.1 K^{-1}, with s_T^* featuring indeed a much more reduced relative error bar compared with T_0.

Some effort has been devoted this last decade to compare different values of S_T reported by different research groups, which were not always consistent with each other.[59] One of the difficulties, when comparing S_T values, is their strong temperature dependence. To fix this problem, one rather considers and compares the S_T^∞ constant ($\lim_{T\to\infty} S_T(T)$), which gives a good estimation of the magnitude of thermophoresis. However, this quantity is not always easy to determine as it requires measurements at a high temperature, where the solute is not always stable. For instance here, the instabilities of the beads (presumably of their molecular coating) were observed above 40 °C prevented us from properly estimating S_T^∞, as discussed above. For this reason, the slope s_T^* looks much more convenient, and just like S_T^∞, s_T^* is also a good reporter of the magnitude of thermophoresis.

Understanding all of the aspects of microscale thermophoresis in liquids in confined environments will require the screening of a large set of parameters, namely, the liquid thickness, the nature of the surface (bare glass, coated glass, or other materials), the nature of the solute (molecules, beads of various diameters, and charges) and the presence/concentration of any salt. For this purpose, the methodology we introduce here is particularly adapted because it allows the acquisition of a full $S_T(T)$ profile in a few minutes, making the task of screening a large set of parameters accessible.

CONCLUSIONS

We introduced an optical methodology aimed at measuring the Soret coefficient of a solute of interest in a given liquid medium. The method is based on the parallel use of wide-field fluorescence microscopy (FM) and quantitative phase microscopy (QPM), FM measuring concentration and QPM measuring temperature. From a single image acquisition, a full set of Soret coefficients for a wide range of temperatures can be measured within a few tens of seconds of acquisition time. Moreover, this dual microscopy approach solves the problem of using two fluorescence probes within the same liquid medium, one for concentration and the other for temperature measurements, a configuration known to yield possible artifacts. It also solves the problem of using high solute concentrations necessary when using beam deflection techniques, leading to possible interparticle interaction effects. We used 0.06 vol % while typical studies rather use 1−2 vol %. The method is further improved by heating gold nanoparticles at their plasmonic resonance in the infrared range and by shaping the laser beam to achieve a perfect temperature linear gradient throughout the fluid layer. The method we introduce here does not suffer from much limitation. In particular, the use of a label-free temperature microscopy does not limit the measurable temperature range,[60] unlike fluorescence-based technique that usually suffers from thermobleaching above 60 °C. This methodology aims at making the screening of parameters involved in microscale thermophoresis in liquids much faster, to enable the study of thermophoresis in liquids at a high temperature and pave the way for broader fundamental research in microscale thermophoresis in liquids and better-controlled applications in nanophotonics involving thermoplasmonic effects.

ASSOCIATED CONTENT

Supporting Information

The Supporting Information is available free of charge at https://pubs.acs.org/doi/10.1021/acs.jpcc.1c06299.

Fabrication of gold nanoparticle samples; photo- and thermobleaching; temperature dependence of fluorescent particles; and temperature retrieval algorithm (PDF)

AUTHOR INFORMATION

Corresponding Author

Guillaume Baffou − *Institut Fresnel, CNRS, Aix Marseille University, Centrale Marseille, 13013 Marseille, France;* orcid.org/0000-0003-0488-1362; Email: guillaume.baffou@fresnel.fr

Authors

Sadman Shakib − *Institut Fresnel, CNRS, Aix Marseille University, Centrale Marseille, 13013 Marseille, France*

Benoit Rogez − *Institut Fresnel, CNRS, Aix Marseille University, Centrale Marseille, 13013 Marseille, France*

Samira Khadir − *Institut Fresnel, CNRS, Aix Marseille University, Centrale Marseille, 13013 Marseille, France*

Julien Polleux − *Department of Ophthalmic Optics, FH Gesundheit, Health University of Applied Sciences Tyrol, 6020 Innsbruck, Austria*

Alois Würger − *Laboratoire Ondes et Matière d'Aquitaine, Université de Bordeaux & CNRS, 33405 Talence, France*

Complete contact information is available at: https://pubs.acs.org/10.1021/acs.jpcc.1c06299

Notes

The authors declare no competing financial interest.

ACKNOWLEDGMENTS

This project received funding from the European Research Council (ERC) under the European Union's Horizon 2020 Research and Innovation Programme (grant agreement no. 772725, project HiPhore).

REFERENCES

(1) Jerabek-Willemsen, M.; Wienken, C. J.; Braun, D.; Baaske, P.; Duhr, S. Molecular Interaction Studies Using Microscale Thermophoresis. *Assay Drug Dev. Technol.* **2011**, *9*, 342−353.

(2) Wienken, C. J.; Baaske, P.; Rothbauer, U.; Braun, D.; Duhr, S. Protein-Binding Assays in Biological Liquids Using Microscale Thermophoresis. *Nat. Commun.* **2010**, *1*, No. 100.

(3) Alexander, C. G.; Jürgens, M. C.; Shepherd, D. A.; Freund, S. M. V.; Ashcroft, A. E.; Ferguson, N. Thermodynamic origins of protein folding, allostery, and capsid formation in the human hepatitis B virus core protein. *Proc. Natl. Acad. Sci. U.S.A.* **2013**, *110*, E2782−E2791.

(4) Alexander, C. G.; Wanner, R.; Johnson, C. M.; Breitsprecher, D.; Winter, G.; Duhr, S.; Baaske, P.; Ferguson, N. Novel microscale approaches for easy, rapid determination of protein stability in academic and commercial settings. *Biochim. Biophys. Acta, Proteins Proteomics* **2014**, *1844*, 2241−2250.

(5) Baffou, G.; Cichos, F.; Quidant, R. Applications and challenges of thermoplasmonics. *Nat. Mater.* **2020**, *19*, 946−958.

(6) Baffou, G. *Thermoplasmonics. Heating Metal Nanoparticles with Light*; Cambridge University Press, 2017.

(7) Robert, H. M. L.; Savatier, J.; Vial, S.; Verghese, J.; Wattellier, B.; Rigneault, H.; Monneret, S.; Polleux, J.; Baffou, G. Photothermal Control of Heat-shock Protein Expression at the Single Cell Level. *Small* **2018**, *14*, No. 1801910.

(8) Braun, M.; Cichos, F. Optically Controlled Thermophoretic Trapping of Single Nano-Objects. *ACS Nano* **2013**, *7*, 11200−11208.

(9) Braun, M.; Würger, A.; Cichos, F. Trapping of SIngle Nano-objects in Dynamic Temperature Fields. *Phys. Chem. Chem. Phys.* **2014**, *16*, 15207.

(10) Braun, M.; Bregulla, A. P.; K, G.; Mertig, M.; Cichos, F. Single Molecules Trapped by Dynamic Inhomogeneous Temperature. *Nano Lett.* **2015**, *15*, 5499−5505.

(11) Liu, Y.; Lin, L.; Bangalore Rajeeva, B.; Jarrett, J. W.; Li, X.; Peng, X.; Kollipara, P.; Yao, K.; Akinwande, D.; Dunn, A. K.; et al. Nanoradiator-Mediated Deterministic Opto-Thermoelectric Manipulation. *ACS Nano* **2018**, *12*, 10383−10392.

(12) Lin, L.; Wang, M.; X, P.; Lissek, E. N.; Z, M.; Scarabelli, L.; Adkins, E.; Coskun, S.; Emrah, H. E.; Unalan; Korgel, B. A.; et al. Opto-thermoelectric nanotweezers. *Nat. Photon.* **2018**, *12*, 195−202.

(13) Lin, L.; Peng, X.; Wang, M.; Scarabelli, L.; Mao, Z.; Liz-Marzán, L. M.; Becker, M. F.; Zheng, Y. Light-Directed Reversible Assembly of Plasmonic Nanoparticles Using Plasmon-Enhanced Thermophoresis. *ACS Nano* **2016**, *10*, 9659−9668.

(14) Enders, M.; Mukai, S.; Uwada, T.; Hashimoto, S. Plasmonic Nanofabrication through Optical Heating. *J. Phys. Chem. C* **2016**, *120*, 6723−6732.

(15) Lin, X.; Si, T.; Wu, Z.; He, Q. Self-thermophoretic motion of controlled assembled micro-/nanomotors. *Phys. Chem. Chem. Phys.* **2017**, *19*, 23606−23613.

(16) Bregulla, A. P.; Cichos, F. Flow fields around pinned self-thermophoretic microswimmers under confinement. *J. Chem. Phys.* **2019**, *151*, No. 044706.

(17) Jiang, Q.; Rogez, B.; Claude, J. B.; Baffou, G.; Wenger, J. Quantifying the Role of the Surfactant and the Thermophoretic Force in Plasmonic Nano-Optical Trapping. *Nano Lett.* **2020**, *20*, 8811−8817.

(18) Makihara, T.; Demers, S. M. E.; Cole, L. E. D.; Zhang, A.; Hafner, J. H. Thermophoresis of gold nanorods from surfaceenhanced Raman scattering and real-time Rayleighscattering in solution. *Anal. Methods* **2019**, *11*, 2482−2488.

(19) Gargiulo, J.; Cerrota, S.; E, C.; Violi, I. L.; Stefani, F. D. Connecting Metallic Nanoparticles by Optical Printing. *Nano Lett.* **2016**, *16*, 1224−1229.

(20) Nicoli, F.; Verschueren, D.; Klein, M.; Dekker, C.; Jonsson, M. P. DNA Translocations through Solid-State Plasmonic Nanopores. *Nano Lett.* **2014**, *14*, 6917−6925.

(21) Yuan, Y.; Lin, Y.; Gu, B.; Panwar, N.; Chuan Tjin, S.; Song, J.; Qu, J.; Yong, K.-T. Optical trapping-assisted SERS platform for chemical and biosensingapplications: Design perspectives. *Coord. Chem. Rev.* **2017**, *339*, 138−152.

(22) Giglio, M.; Vendramini, A. Thermal-Diffusion Measurements near a Consolute Critical Point. *Phys. Rev. Lett.* **1975**, *34*, 561−564.

(23) Putnam, S. A.; Cahill, D. G. Micron-Scale Apparatus for Measurements of Thermodiffusion in Liquids. *Rev. Sci. Instrum.* **2004**, *75*, 2368−2372.

(24) Putnam, S. A.; Cahill, D. G. Transport of Nanoscale Latex Beads in a Temperature Gradient. *Langmuir* **2005**, *21*, 5317−5323.

(25) Putnam, S. A.; Cahill, D. G.; Wong, G. C. L. Temperature Dependence of Thermodiffusion in Aqueous Suspensions of Charged Nanoparticles. *Langmuir* **2007**, *23*, 9221−9228.

(26) Köhler, W. Thermodiffusion in polymer solutions as observed by forced Rayleigh scattering. *J. Chem. Phys.* **1993**, *98*, 660−668.

(27) Wiegand, S.; Ning, H.; Kriegs, H. Thermal diffusion forced Rayleigh scattering setup optimized for aqueous mixtures. *J. Phys. Chem. B* **2007**, *111*, 14169−14174.

(28) Rauch, J.; Köhler, W. Diffusion and Thermal Diffusion of Semidilute to Concentrated Solutions of Polystyrene in Toluene in the Vicinity of the Glass Transition. *Phys. Rev. Lett.* **2002**, *88*, No. 185901.

(29) Ning, H.; Buitenhuis, J.; Dhont, J. K. G.; Wiegand, S. Thermal Diffusion Behavior of Hard-Sphere Suspensions. *J. Chem. Phys.* **2006**, *125*, No. 204911.

(30) Rusconi, R.; Isa, L.; Piazza, R. Thermal-Lensing Measurement of Particle Thermophoresis in Aqueous Dispersions. *J. Opt. Soc. Am. B* **2004**, *21*, 605−616.

(31) Braun, D.; Libchaber, A. Trapping of DNA Thermophoretic Depletion and Convection. *Phys. Rev. Lett.* **2002**, *89*, No. 188103.

(32) Duhr, S.; Arduini, S.; Braun, D. Thermophoresis of DNA Determined by Microfluidic Fluorescence. *Eur. Phys. J. E* **2004**, *15*, 277−286.

(33) Duhr, S.; Braun, D. Thermophoretic Depletion Follows Boltzmann Distribution. *Phys. Rev. Lett.* **2006**, *96*, No. 168301.

(34) Wiegand, S. TOPICAL REVIEW: Thermal diffusion in liquid mixtures and polymer solutions. *J. Phys. Cond. Mat.* **2004**, *16*, R357−R379.

(35) Iacopini, S.; et al. The "macromolecular tourist": Universal temperature dependence of thermal diffusion in aqueous colloidal suspensions. *Eur. Phys. J. E* **2006**, *19*, 59−67.

(36) Niether, D.; Wiegand, S. Thermophoresis of biological and biocompatible compounds in aqueous solution. *J. Phys. Cond. Mat.* **2019**, *31*, No. 503003.

(37) Jiang, H.-R.; Wada, H.; Yoshinaga, N.; Sano, M. Manipulation of Colloids by a Nonequilibrium Depletion Force in a Temperature Gradient. *Phys. Rev. Lett.* **2009**, *102*, No. 208301.

(38) Vigolo, D.; Buzzaccaro, S.; Piazza, R. Thermophoresis and Thermoelectricity in Surfactant Solutions. *Langmuir* **2010**, *26*, 7792−7801.

(39) Eslahian, K. A.; Majee, A.; Maskos, M.; Würger, A. Specific salt effects on thermophoresis of charged colloids. *Soft Matter* **2014**, *10*, 1931−1936.

(40) Iacopini, S.; Piazza, R. Thermophoresis in Protein Solutions. *Europhys. Lett.* **2003**, *63*, 247−253.

(41) Anderson, J. L. Colloid Transport by Interfacial Forces. *Annu. Rev. Fluid Mech.* **1989**, *21*, 61−99.

(42) Fu, L.; Merabia, S.; Joly, L. What Controls Thermo-osmosis? Molecular Simulations Show the Critical Role of Interfacial Hydrodynamics. *Phys. Rev. Lett.* **2017**, *119*, No. 214501.

(43) Ganti, R.; Liu, Y.; Frenkel, D. Molecular Simulation of Thermo-osmotic Slip. *Phys. Rev. Lett.* **2017**, *119*, No. 038002.

(44) Bregulla, A. P.; Würger, A.; Günther, K.; Mertig, M.; Cichos, F. Thermo-Osmotic Flow in Thin Films. *Phys. Rev. Lett.* **2016**, *116*, No. 188303.

(45) Würger, A. Thermal Non-Equilibrium Transport in Colloids. *Rep. Prog. Phys.* **2010**, *73*, No. 126601.

(46) Velghe, S.; Primot, J.; Guérineau, N.; Cohen, M.; Wattellier, B. Wavefront Reconstruction from Multidirectional Phase Derivatives

https://doi.org/10.1021/acs.jpcc.1c06299
J. Phys. Chem. C 2021, 125, 21533−21542

Generated by Multilateral Shearing Interferometers. *Opt. Lett.* **2005**, *30*, 245−247.
(47) Bon, P.; Maucort, G.; Wattellier, B.; Monneret, S. Quadriwave lateral shearing interferometry for quantitative phase microscopy of living cells. *Opt. Express* **2009**, *17*, 13080−13094.
(48) Baffou, G. Quantitative phase microscopy using quadriwave lateral shearing interferometry (QLSI): principle, terminology, algorithm and grating shadow description. *J. Phys. D: Appl. Phys.* **2021**, *54*, No. 294002.
(49) Kundrat, F.; Baffou, G.; Polleux, J. Shaping and Patterning Gold Nanoparticles via Micelle Templated Photochemistry. *Nanoscale* **2015**, *7*, 15814−15821.
(50) Weinert, F. M.; Braun, D. An Optical Conveyor for Molecules. *Nano Lett.* **2009**, *9*, 4264−4267.
(51) Baffou, G.; Berto, P.; Bermúdez Ureña, E.; Quidant, R.; Monneret, S.; Polleux, J.; Rigneault, H. Photoinduced Heating of Nanoparticle Arrays. *ACS Nano* **2013**, *7*, 6478−6488.
(52) Harris, R. M. Light microscopic depth measurements of thick sections. *J. Neuro. Meth.* **1985**, *14*, 97−100.
(53) Durdevic, L.; Robert, H. M. L.; Wattellier, B.; Monneret, S.; Baffou, G. Microscale Temperature Shaping Using Spatial Light Modulation on Gold Nanoparticles. *Sci. Rep.* **2019**, *9*, No. 4644.
(54) Liu, C.; Tessier, G.; Esparza, S. I. F.; Guillon, M.; Berto, P. Reconfigurable Temperature Control at the Microscale by Light Shaping. *ACS Photonics* **2019**, *6*, 422−428.
(55) Baffou, G.; Bermúdez Ureña, E.; Berto, P.; Monneret, S.; Quidant, R.; Rigneault, H. Deterministic Temperature Shaping using Plasmonic Nanoparticle Assemblies. *Nanoscale* **2014**, *6*, 8984−8989.
(56) Baffou, G.; Bon, P.; Savatier, J.; Polleux, J.; Zhu, M.; Merlin, M.; Rigneault, H.; Monneret, S. Thermal Imaging of Nanostructures by Quantitative Optical Phase Analysis. *ACS Nano* **2012**, *6*, 2452−2458.
(57) Thormählen, I.; Straub, J.; Grigull, U. Refractive index of water and its dependence on wavelength, temperature and density. *J. Phys. Chem. Ref. Data* **1985**, *14*, 933−945.
(58) Radhakrishnan, R.; Gallais, L.; Monneret, S. Wavefront sensing applied to determine the temperature dependence of the refractive index of liquids. *Appl. Opt.* **2019**, *58*, 3646−3651.
(59) Würger, A. Hydrodynamic Boundary Effects on Thermophoresis of Confined Colloids. *Phys. Rev. Lett.* **2016**, *116*, No. 138302.
(60) Baffou, G.; Polleux, J.; Rigneault, H.; Monneret, S. Super-Heating and Micro-Bubble Generation around Plasmonic Nanoparticles under cw Illumination. *J. Phys. Chem. C* **2014**, *118*, 4890.

https://doi.org/10.1021/acs.jpcc.1c06299
J. Phys. Chem. C 2021, 125, 21533−21542